Published in final edited form as:
Structure. 2009 February 13; 17(2): 190–201. doi:10.1016/j.str.2008.12.013.

Structural Analysis of Ligand Stimulation of the Histidine Kinase NarX

Jonah Cheung[1] and **Wayne A. Hendrickson**[1,2,‡]

[1] Department of Biochemistry and Molecular Biophysics, Columbia University, New York, NY 10032, USA

[2] Howard Hughes Medical Institute, Columbia University, New York, NY 10032, USA

SUMMARY

Histidine kinase receptors are a large family of membrane-spanning proteins found in many prokaryotes and some eukaryotes. They are a part of two-component signal transduction systems, which each comprise a sensor kinase and a response regulator and are involved with the regulation of many cellular processes. NarX is a histidine kinase receptor that responds to nitrate and nitrite to effect regulation of anaerobic respiration in various bacteria. We present high resolution x-ray crystal structures of the periplasmic sensor domain from *Escherichia coli* NarX in a complex with nitrate and in the apo state. Our analysis reveals that nitrate-binding induces conformation changes that result in a piston-type displacement between the N- and C-terminal helices of the periplasmic domain. Such conformational changes might represent a conserved mechanism of signaling in histidine kinases by which ligand binding is communicated across the lipid bilayer.

Keywords

Four-helix bundle; Nitrate; Selenomethionyl MAD; Signal transduction

INTRODUCTION

To ensure survival, bacteria must adapt to changing external environmental conditions. Two-component signal transduction pathways allow bacteria to couple changes in the extracellular environment to an internal response. Over the last decade, many of such pathways have been found, universally in prokaryotes and also in eukaryotes such as yeast and plants, but not in metazoan animals (Stock et al., 2000; West and Stock, 2001). Typical two-component systems consist of a sensor histidine kinase and its paired response regulator, which interact in tandem to relay an external stimulus, often from a small molecule ligand, across the periplasmic membrane to effectors in the cytoplasm. Typical histidine kinases are homodimeric transmembrane proteins composed of a modular extracellular domain and a conserved cytoplasmic kinase domain (Wolanin et al., 2002). Upon detection of a signal, changes within the sensor domain are coupled to a

‡Correspondence: Wayne A. Hendrickson, Department of Biochemistry and Molecular Biophysics, Columbia University, New York, NY, 10032. E-mail: wayne@convex.hhmi.columbia.edu; Tel. 212-305-3456; Fax. 212-205-7379.

ACCESSION NUMBERS

Atomic coordinates and structure factors (codes 3EZH and 3EZI) have been deposited in the Protein Data Bank (http://www/rcsb/pdb).

phosphotransfer cascade that ultimately affects the state of the effector domain of the response regulator. Sensory stimulation typically leads to ATP-dependent autophosphorylation of a conserved histidine residue in the sensor protein and subsequent transfer of the phosphoryl group to an aspartate residue in the regulatory domain of the cognate response regulator (Dutta et al., 1999), but in some instances stimulation leads to dephosphorylation of the response regulator (Russo and Silhavy, 1993). The state of phosphorylation of the response regulator modulates the activity of its effector domain, often a transcriptional repressor, which then leads to an adaptive cellular response (Robinson et al., 2000).

In this study, part of a larger project aimed at understanding how signals are transferred across membranes by sensor histidine kinases, we analyze the sensor domain structure of the nitrate-responsive histidine kinase NarX. The NarX-NarL two-component system is involved in the control of anaerobic respiration and is responsive to both nitrate and nitrite, although exhibiting a stronger response to nitrate (Lee et al., 1999). The response regulator NarL is a transcription factor, and upon phosphorylation it activates the gene cluster for nitrate reductase (*narGHJI*) but represses those for fumarate reductase (*fdrABCD*) and dimethyl sulfoxide reductase (*dmsABC*) (Iuchi and Lin, 1991; Schroder et al., 1994; Stewart, 1993). By increasing expression of genes involved in nitrate respiration and decreasing expression of genes involved in alternate respiration pathways, the cell is able to increase its efficiency for utilizing nitrate as an electron acceptor in anaerobic conditions. More recently it has also been shown that phosphorylated NarL also activates an aspartate-ammonia lyase (*aspA*), the DcuS-DcuR two-component system (*dcuSR*) (Goh et al., 2005), as well as proteins of unknown function (*yeaR-yoaG*) (Lin et al., 2007). NarX displays 32% amino acid identity with NarQ, a homologous nitrate sensor of the NarQ-NarP pair. NarQ is able to phosphorylate NarL at a faster rate than NarX, but it exhibits a much slower phosphatase activity (Schroder et al., 1994). NarL and NarP also have different specificities for the various downstream target operons (Kaiser and Sawers, 1995).

The periplasmic sensor domain of NarX (residues 43 - 148) is flanked by two hydrophobic transmembrane regions (residues 15 - 42 and 149 - 171). Mutational analyses of conserved residues in the “P-box” region (residues 43 - 60) of the sensor domain suggest that some of these residues are involved with ligand binding (Cavicchioli et al., 1996). The linker region (residues 181 - 233), found in many sensor kinases, follows the second transmembrane region and is thought to be composed of two short amphipathic α-helices involved with transmission of a signal from the sensor to the kinase domain (Appleman et al., 2003). Unique to NarX and NarQ sensors is a cysteine rich central region (residues 227 - 387 of NarX) lying between the linker and the kinase domain, but mutational evidence has not shown a critical role for the cysteine residues in signaling (Stewart, 2003).

Although numerous genetic and mutational studies have been performed, no structural information for NarX has been published to date. Here we report crystal structures of the NarX sensor domain in complex with nitrate and in its apo state. We expressed and purified the recombinant sensor domain from *Escherichia coli* as a soluble protein, and structures were solved in the presence of nitrate and in the apo state by x-ray crystallography. The NarX sensor is found to be dimeric in the ligated state in crystals, despite the lack of observable association of this molecular fragment in solution. Conformational changes that occur upon nitrate binding are analyzed in relation to the mechanism of signal transduction through the plasma membrane.

RESULTS

Overall Structure and Topology

We used multiwavelength anomalous diffraction (MAD) at the Se K-edge to determine the structure of $NarX_{S1}$ (sensor domain residues 38 – 151) in complex with nitrate at 1.7Å resolution from a single crystal of the selenomethionyl (SeMet) protein (Table 1). Two polypeptide units were found in the asymmetric unit as an apparent molecular dimer, and we refer to the protomers as A and A′. Each protomer is fully ordered from residue 42 through residue 151, and electron density corresponding to the linker segment from a polyhistidine-tagged fusion construct could also be observed to varying degrees. Positions through 155 and 154′ were included in the final refinement of the structure. A total of 227 residues, 255 water molecules, and 1 nitrate ion were refined against a high-angle dataset taken at the edge wavelength (Table 2) to R and R_{free} values of 21.7% and 25.8% respectively.

The structure of $NarX_S$ (Figs. 1A and 1B) is best described as a dimer of four-helix bundles, related by a quasi two-fold axis of symmetry running roughly parallel to the long axes of the helices. The protomers of this dimer are very similar (rmsd on Cα = 0.71Å). We name the four helices of each subunit H1 to H4 and H1′ to H4′ respectively. The first helix spans residues 43 to 62 of each protomer. Each of the second, third, and fourth helices contain short breaks that divide each into two shorter subhelices. Helix H2/H2′ contains a kink at residues 82 and 83, dividing it into H2a/H2a′ (residues 68 - 81) and H2b/H2b′ (residues 84 - 93); helix H3/H3′ contains a bulge-forming insertion at residue 109, which dividing it into H3a/H3a′ (residues 96 -108) and H3b/H3b′ (residues 110 - 116); and Helix H4/H4′ contains a turn at position 123, dividing it into H4a/H4a′ (residues 120 - 122) and H4b/H4b′ (124 - 151). Both H1/H1′ and H4/H4′ are slightly curved in nature, but run roughly parallel to each other, while the other helices appear to be oriented at more of an angle to one another.

Nitrate binding in $NarX_S$

Clear electron density was found for a single nitrate ion partially buried within the dimer interface, between H1 and H1′ (Fig. 1A and Fig. 2) in the conserved P-box region (Cavicchioli et al., 1996; Stewart, 2003) of the protein. This single ligand-binding site between NarX protomers contrasts with the situation in Tar where each subunit contains a potential ligand binding site, but the allosteric binding of aspartate to only one site suffices to elicit a signaling state of the receptor (Yeh et al., 1996). The orientation of the nitrate ion is such that one nitrogen-oxygen bond is aligned with the quasi two-fold rotation axis of the dimer; consequently one of its three oxygen atoms is located on-axis while the other two lie off-axis. The nitrate ion is flanked on either side by Arg54 and Arg54′, which make hydrogen bonds to the two off-axial oxygen atoms of nitrate via their Nε atoms and to the axial oxygen atom via each $N\eta^2$ atom. The carbonyl oxygen atoms of Gly51 and Gly51′ lie on either side of the nitrogen atom of nitrate and make short van der Waals contact at 2.7Å and 2.8Å, respectively. A water molecule found within hydrogen bonding distance from the carbonyl oxygen of Ile47′ is located essentially equidistant from the axial nitrate oxygen (3.26Å) and the carbonyl oxygen of Ile47 (3.25Å). These distances are slightly beyond the optimal hydrogen bonding range of 2.7 to 3.2Å. We believe that the refined water site is probably an average of two mutually exclusive states, one optimally hydrogen-bonded to the carbonyl oxygen of Ile47 and the other optimally to the axial oxygen of nitrate.

Similarities of NarX with Other Structures

A search of the structural database using the Dali server (Holm and Sander, 1993) has shown high structural similarity (Z >7.5) with other four-helix bundle proteins of similar topology such as the oxygen-carrier myohemerythrin (Sheriff et al., 1987) and the aspartate

receptor Tar (Yeh et al., 1996). Because of the high structural and functional similarity between $NarX_S$ and Tar, we present a structure-based sequence alignment (Fig. 3) of these periplasmic domains, from which 67 of 114 Cα positions superimpose with a root mean square deviation of 1.9 Å. We also include the periplasmic domain sequences of NarX and NarQ from other organisms as sequence aligned to the *E. coli* NarX periplasmic domain sequence using ClustalW (Thompson et al., 1994). It is evident that in contrast to the relatively high sequence similarities between the NarX homologs (23.7% to 73.9% pairwise identity), Tar is quite dissimilar (7.3% identity with *E. coli* NarX). Despite structural similarities, $NarX_{S1}$ and Tar are diverged beyond sequence recognition if they are indeed homologs.

Differences between the structures of $NarX_{S1}(NO_3)$ and Tar lie in helix lengths, helix curvatures, and inter-helical loops. Helix H1 of $NarX_S$ is shorter and more curved than α1 of Tar. The loop in $NarX_S$ that corresponds to the extended nine-residue loop between α1 and α2 in Tar, which contains residues involved with its ligand binding (Yeh et al., 1996), is shorter. Helix H2a of $NarX_S$ is relatively straight and follows α2 of Tar but is shorter in length as well. Tar lacks a helix corresponding to H2b of $NarX_S$ but instead contains a six-residue loop between α2 and α3. Helix α3 of Tar is longer than H3 of $NarX_S$ and lacks an insertion that consequently throws residues in H3a of $NarX_S$ out of alignment with some residues of α3 in Tar. Helix H4 of $NarX_S$ is similar in length to α4 of Tar but is more curved. Because helices in Tar tend to be straighter and longer than those in $NarX_S$, Tar protomers have a more elongated overall shape than $NarX_S$ (Fig. 4).

Dimerization

The dimer interface of $NarX_S(NO_3)$ buries a combined total of 1926Å^2 in accessible surface area from the two subunits (rotation X = 177.3°, screw translation t_X = −0.103Å) (Hendrickson, 1979). This interfacial area is somewhat higher than in Tar (1699Å^2, Yeh et al., 1996) or in a functional dimer of PhoQ (1528Å^2, Cheung et al., 2008) and a similar DcuS dimer (1684Å^2, Cheung & Hendrickson, 2008). Most of the interactions at the dimer interface in $NarX_S$ are between residues of the highly conserved P-box region (Fig. 3), located on H1 and H1′ and centered at the nitrate-binding site. Inter-subunit hydrogen bonds are formed between Arg54 side chains and the Oδ and carbonyl oxygen atoms of Asn48′, and reciprocally between Arg54′ and Asn48. In addition, reciprocal van der Waals contacts join residues at the beginnings of H1/H1′ and ends of H4′/H4 and with residues in loops H1-H2/H1′-H2 and in loops H3′-H4′/H3-H4.

The orientation of the two NarX subunits with respect to each other is similar to that of Tar, but there is a small difference. If one protomer from the $NarX_S(NO_3)$ dimer is superimposed onto one from the Tar dimer, a rotation of 9.3° is needed to superimpose the $NarX_S$ dimer mate onto the respective Tar dimer mate to generate the new ‘Tar-like’ dimer. The axis of rotation passes through the middle of the fourth helix in $NarX_S$ and almost intersects the quasi two-fold rotation axis of the dimer, lying roughly orthogonal to it (Fig. 4). These orientational differences are slight and might be affected by connections to transmembrane helices in the intact proteins.

Ligand-free NarX

The structure of $NarX_{S2}$ (residues 42-148) in the apo state (Fig. 5) was solved by molecular replacement with four molecules (A, B, C, and D) in the asymmetric unit. Two electron-density features in proximity to crystal contacts were modeled in as isopropanol, which was present in the crystallization buffer although not an absolute requirement for obtaining crystals. Together with 438 water molecules and 2 isopropanol molecules, 406 residues of

$NarX_{S2}$(apo) have been refined to 1.7Å to a final R and R_{free} of 18.9% and 23.9%, respectively (Table 2).

The four molecules in the asymmetric unit of $NarX_{S2}$(apo) appear to form a pair of pairs. Molecules A and B contact each other in a similar way as for C and D. Residues lying on H2 of molecule A contact residues on H3 of molecule B, and likewise between molecules C and D. Molecule B and C contact each other in a different manner, mainly between residues of H1 in each. All of the interfaces are small and not related to those in the complex with nitrate.

Structural Deviations within $NarX_S(NO_3)$ and $NarX_S$(apo)

The presence of multiple molecules in the asymmetric unit in the structures of $NarX_{S1}(NO_3)$ and $NarX_{S2}$(apo) allows discrimination between genuine structural changes associated with binding of the nitrate ligand and irrelevant differences such ones that might be due to lattice packing interactions. We thus identified regions of structural invariance within molecules of each state, at a conservative 3σ level, using error-scaled difference distance matrices generated by ESCET (Schneider, 2000; Schneider, 2002). We then used only these invariant regions in each state as the basis for superimposition. Corresponding Cα positions were superimposed in LSQMAN (Kleywegt and Jones, 1994) in a combinatorial pairwise manner for all molecules within a given state. After these superpositions, the averaged Cα deviations were found over the entire span of each state (Fig. 6). With exception of some residues at the N- and C-termini, structural variations are small at less than 0.5Å on average. The largest of structural differences within a state are at the C-terminal ends of helix H4b in the nitrate-bound structure, from residue 144 and onward. These helices extend away from the body of $NarX_{S1}(NO_3)$ and are involved in lattice contacts with neighboring molecules.

Conformational Differences between the Two States

In order to understand structural differences between the nitrate-bound and apo state of the NarX sensor domain, we first identified a conformationally invariant region (residues 83 to 106) common to all molecules of both states as a reference point against which to compare differences. This analysis was done using ESCET (Schneider, 2000; Schneider, 2002) as before and results are reflected in the difference distance matrix (Fig. 7). All molecules of the apo state were superimposed pairwise onto each molecule of the nitrate-bound state using the identified conformationally invariant Cα positions, and the averaged Cα deviations between corresponding positions were plotted against residue number (Fig. 6). The averaged structural differences between the nitrate-bound and apo state are much greater than those within each state, and they cannot be attributed to crystal packing.

Conformational differences between the nitrate-bound and apo states can be directly visualized by superimposition of molecules from each state by least squares minimization of the conformationally invariant Cα positions of residues 83 to 106. These differences are best described as a ‘hinging’ movement at junctures from helices H2a to H2b and from H3b to H3a, respectively (Fig. 8A). This results in a differential tilting between H4 and H1 such that H1 is displaced relative to H4 along the long axis of the helices. These changes happen without repacking of interfacial sidechains, however. The consequences of such movements are best appreciated in a dimeric context, whereby a hypothetical apo dimer is constructed by superimposition of apo state monomers upon each protomer of the nitrate-bound state. Then, relative to the apo state, helices H2a and H3b are displaced towards the plane of the dimer interface upon nitrate binding, and there is a piston-like displacement of H1 helices, relative to H4 helices, by ~1Å towards the plane of the putative membrane (Fig. 8B).

Conformational Changes at the Ligand-Binding Site

The binding of nitrate appears to induce local conformational changes of H1 residues in the vicinity of the binding site. In particular, Arg54 adopts alternative confomations in the two states. In the apo state, the side chain of Arg54 turns inward and is hydrogen bonded to a carboxylate oxygen of Glu135. In the nitrate-bound dimer, the side chains of Arg54 and Arg54′ are oriented towards the apposed protomers and make inter-subunit hydrogen bonds to the backbone carbonyls and the side chain oxygen atoms of Asn48′ and Asn48, respectively. In the apo state, residues in H1 above and below the nitrate binding site assume a relatively straight α-helical conformation. In the nitrate-bound state, there is a distortion of H1/H1′ at residues below Gly51/Gly51′ such that the lower portion of each helix is bent towards the opposite protomer, and the hydrogen bonding patterns between residues on successive turns become more similar to that of a 3_{10}-helix. The hydrogen bonding in this region of the nitrate-bound state involves bifurcated interactions to carbonyl i from amides i +3 and i+4, whereas those of the apo state are strictly between residues i and i+4. Resulting distortions in the ligated state increase the helical pitch of the lower portion of H1 and H1′, which contributes to the relative displacement of N-termini towards the putative plane of the membrane.

DISCUSSION

The high resolution structures that we present for the periplasmic sensor domain of NarX in the apo state and nitrate-bound state reveal a four helix bundle. The all helical fold is similar to that of the aspartate receptor Tar (Yeh et al., 1996), but different from histidine kinase sensor domains of similar size such as PhoQ (Cho et al., 2006), CitA (Reinelt et al., 2003), and DcuS (Pappalardo et al., 2003), all of which have the PhoQ/DcuS/CitA (PDC) sensor fold (Cheung et al., 2008). Unique to NarX is the location of a single ligand binding site at the dimer interface, involving residues of both protomers.

Histidine kinase receptors are thought to function in the context of a dimer in the cell membrane (Wolanin et al., 2002), and similarities between the NarX dimer in our nitrate-bound state and the Tar dimer (Yeh et al., 1996) suggest biological relevance for this dimer. Nevertheless, $NarX_{S1}$ remains monomeric in solution even at protein concentrations up to 10mM in the presence of excess nitrate, when analyzed by equilibrium sedimentation ultracentrifugation at physiological conditions (data not shown). What is not physiological about this experiment is the absence of membrane association. We believe that the ability of the NarX periplasmic domain to dimerize on its own is reduced when expressed in absence of its cognate transmembrane and cytoplasmic domains. Theoretically, the likelihood of a membrane-tethered protein to associate has been shown to be 10^6-fold greater than when tumbling freely in solution (Grasberger et al., 1986; Metzger, 1992). Apparently authentic dimerization was likely promoted here by high protein concentrations in the crystal (55mM).

The role of Arg54 in nitrate binding is consistent with biochemical and genetic studies of NarX (Cavicchioli et al., 1996; Chiang et al., 1997; Stewart, 2003; Williams and Stewart, 1997). The coordination of nitrate by the side chains of Arg54 and Arg54′ is through direct hydrogen bonding, and contrasts with aspartate binding by Tar where interactions between protein and ligand involve indirect water-mediated hydrogen bonding (Yeh et al., 1996). The binding of nitrate to NarX is also quasi-symmetric, and contrasts with the asymmetric binding of aspartate to Tar in which only one of the two binding sites is fully occupied (Yeh et al., 1996). Although binding of a single water molecule at the nitrate-binding site appears to be asymmetric, it is difficult to determine the consequence of its effect on the rest of the structure.

The binding site of NarX readily accommodates nitrite as well as nitrate, perhaps in multiple poses, which is consistent with redundant binding characteristics (Lee et al., 1999). NarX also responds to the non-planar sulfite ion (Williams and Stewart, 1997), which may indicate a certain plasticity at the ligand binding site and dimer interface. Other anions such as ClO_3^-, MoO_4^{2-}, WO_4^{2-}, SeO_3^{2-}, BrO_3^-, HCO_3^-, SO_4^{2-} and HPO_4^{2-} have no measurable activation effect on NarX (Williams and Stewart, 1997), and are likely to be excluded from the binding site in part by steric conflicts with the carbonyl oxygen atoms of Gly51 and Gly51′, which lie 5.49Å apart, or because they cannot satisfy proper hydrogen bonding requirements. Single-residue substitutions in NarX, mostly in the P-box region of H1, result in altered signaling phenotypes (Williams and Stewart, 1997). Such results indicate that in addition to the residues involved with ligand binding, wild-type NarX signaling is highly sensitive to disruptions in the conformation and packing of the helices at the dimer interface and in the region proximal to the putative plane of the membrane.

The location of a single ligand-binding site within a conserved region of the dimer interface suggests a role of ligand binding in dimer stabilization. Although histidine kinases function as dimers, and it is presumed that NarX exists as a dimer within the membrane in the apo state, the stability of the periplasmic dimer interface in the apo state is unknown. Our inability to detect self-association of the NarX sensor domain by sedimentation equilibrium ultracentrifugation, even in the presence of nitrate at very high protein concentrations, suggests that the intrinsic affinity for self-association is relatively weak. We believe that the conformational differences observed between the nitrate-bound and apo state are likely the concerted result of both ligand binding and increased dimeric interactions. In the absence of nitrate, the periplasmic domain of NarX crystallizes as a monomer, but in such a way that the ligand binding site remains accessible. Soaking of nitrate into these crystals fails to cause cracking, which suggests that the binding of nitrate alone does not suffice for all the structural changes observed between the two states. Lattice disruption would be expected from the $NarX_S(NO_3)$ conformation. Of course, lattice interactions might resist such disruption but the contact interfaces appear to be weak. It seems more likely that nitrate can only bind to NarX when two protomers are favorably disposed in a dimeric arrangement. We believe that when NarX is in its native apo state, with the sensor domain anchored to its dimeric transmembrane domain, ligand binding causes local conformational changes that reinforce the dimer interface between sensor domains. The side chains of Arg54/Arg54′ are repositioned by their binding to nitrate in a way that allows inter-subunit hydrogen bonding to N48′/N48, respectively. The dimer interface is thus stabilized by ligand binding, resulting in conformational changes that displace H1 with respect to H4 towards the putative plane of the membrane.

The conformational changes that occur within the periplasmic domain of NarX upon binding of nitrate are reminiscent of those in Tar, in which a ~1Å displacement between the N- and C-terminal helices of the periplasmic domain also occurs upon ligand binding (Chervitz and Falke, 1996; Ottemann et al., 1999; Falke and Hazelbauer, 2001). It should be noted that in our case such results were obtained from crystals grown at 4°C, and the structural changes occurring at physiological temperatures may be different. Such helix displacements are of relatively low energy, requiring only side-chain conformational adjustments along inter-helical interfaces (Chothia and Lesk, 1985) and mutations along H1 that result in signaling defects in NarX (Williams and Stewart, 1997; Appleman et al., 2003) may perturb inter-helical contacts and alter the extent to which the proper conformational changes can occur. It is important to note that there are distinct differences between the conformational changes that take place in NarX and Tar upon ligand binding. The conformational changes in NarX occur symmetrically between the two protomers as the binding of nitrate is symmetric, while in Tar they appear to be localized to only one subunit due to asymmetric aspartate binding (Biemann and Koshland, 1994; Chervitz and Falke, 1996; Falke and Hazelbauer, 2001). In

addition, the relative displacement between the N- and C-terminal helices of the NarX sensor domain is opposite in direction to that of the Tar sensor domain.

The opposite directionality in conformational changes on ligand binding correlates with differences in Tar and NarX function. A downward displacement of the N-terminal helix in NarX occurs upon nitrate binding, which contrasts with a downward displacement of the C-terminal helix, within only one subunit in Tar, upon aspartate binding (Chervitz and Falke, 1996; Falke and Hazelbauer, 2001). These opposing directions of helix displacements between the two receptors are reflected in differences of signaling responses; ligand binding in NarX promotes the phosphorylated signaling state but ligand binding in *Salmonella typhimurium* Tar gives an attractant response, which by analyses of chimeric proteins seems to correspond to promotion of dephosphorylation. Histidine kinase sensors and chemotactic receptors are sufficiently parallel that functional chimeric receptors can be constructed from components of each (Utsumi et al., 1989), and this approach has been taken in NarX-chemoreceptor fusions (Ward et al., 2002; Xu et al., 2005; Ward et al., 2006; Xu et al., 2007). One of these, the NarX-Tar (Tart) chimeric protein, is directly relevant here. Tart is a fusion of the NarX periplasmic sensor domain with the Tar cytoplasmic signaling domain, and it is shown to be sensitive to nitrate and nitrite as repellants (Ward et al., 2002). This reversal from the attractant response of Tar to aspartate is consistent with our observation of oppositely directed transmembrane displacement in NarX compared with Tar. It should be noted, however, that directionality of sensory response is not an intrinsic property of Tar-like receptors. McpB is a Tar-receptor homolog in *Bacillus subtilis* that responds to asparagine to activate CheA whereas Tar inactivates CheA (Garrity and Ordal, 1997; Szurmant et al., 2004).

Our studies reveal a possible conserved signaling mechanism between histidine kinase and chemotaxis sensors as piston-type displacement, on the order of about 1Å, between the N- and C-terminal helices of the periplasmic domain. Such a displacement must be transmitted through the transmembrane helices in order to reach the cytoplasmic domain. At this point it is unknown whether the same vectors of motion are retained upon entry into the cytoplasmic domain, or whether such motions are converted into twisting or torqueing motions within the transmembrane region en route to the cytoplasm. Further work is necessary to determine exactly how piston-type displacements between the N- and C-terminal helices of periplasmic sensor domains trigger conformational changes in the cytoplasmic histidine kinase domains.

EXPERIMENTAL PROCEDURES

Cloning

A DNA fragment corresponding to residues 38 to 151 of NarX ($NarX_{S1}$) was amplified from genomic DNA of *E. coli K-12* (ATCC Bioproducts) using 5′ and 3′ primers containing Nde1 and Not1 restriction sites respectively. The fragment was ligated into the pET22b+ expression vector (Novagen) between the Nde1 and Not1 sites of the polylinker region. The resulting construct was used for isopropyl-β-D-thiogalactopyranoside (IPTG)-inducible cytoplasmic expression of $NarX_{S1}$ as a fusion protein, containing a hexahistidine tag on the C-terminus separated by a five residue linker of the amino acid sequence “AAALE”.

Based on ordered residues of the nitrate-bound structure, a shorter DNA fragment corresponding to residues 44 to 148 of NarX was amplified from the pET22b+ $NarX_{S1}$ construct using the appropriate primers, and ligated into the pGEX-4T-2 expression vector (Amersham Pharmacia Biotech) between the BamH1 and EcoR1 cloning sites. A stop codon was engineered immediately following the last residue of the construct, allowing IPTG-inducible cytoplasmic expression of NarX 44-148 as an N-terminal glutathione S-transferase (GST)-fusion protein. Within the construct lies an internal thrombin cleavage site, which

upon cleavage leaves an extra glycine and serine on the N-terminus of NarX 44-148. Because the two residues left behind are identical to residues 42 and 43 of the native NarX sequence, the resulting purified protein is effectively $NarX_{S2}$ (NarX 42-148).

Expression and Purification

Selenomethionyl (SeMet) $NarX_{S1}$ was expressed from Novagen *E. coli* BL21 (DE3) cells, grown in 4L of selenomethionine minimal media at 37°C to an optical density (OD) of 0.6, after being inoculated 1:100 from an overnight culture grown from minimal media. Expression was induced using IPTG at 1mM for 3 hours at 30°C. The cells were harvested and resuspended in 50mM Tris-HCl pH 8.0 and 100mM NaCl. Cell supernatant was prepared by sonication, cleared by centrifugation, and then passed through a 5ml HiTrap™ Chelating column (Pharmacia) previously equilibrated with Ni^{2+}. The protein was eluted from the column using an imidazole gradient and then further purified using a MonoQ™ 10/10 column (Pharmacia) over a shallow salt gradient. The protein was dialyzed into storage buffer (20mM N-2-hydroxyethylpiperazine-N′-2-ethanesulfonate (HEPES) pH 8.0, 50mM NaCl, 1mM EDTA) and concentrated to ~16mg/ml. The protein appeared homogenous by SDS-PAGE and native PAGE, and appeared to be monomeric by gel filtration chromatography in comparison to protein molecular weight standards. Full incorporation of selenomethionine into the expressed protein was confirmed by mass spectrometry (data not shown).

$NarX_{S2}$ was expressed at 30°C for 3 hours with 1mM IPTG from a 2L culture of *E. coli* BL21 (DE3) cells (Novagen) in Luria-Bertani (LB) media. Induction began upon reaching an OD of ~0.6 following a 1:100 inoculation from an overnight culture grown in LB media at 37°C. The cells were harvested and resuspended in phosphate buffered saline (PBS) pH 7.4 and 5mM dithiolthreitol (DTT). Cell supernatant was prepared by sonication, cleared by centrifugation, and then passed through a hand-poured 8mL glutathione Sepharose™ 4B (Pharmacia) gravity column. The column was washed with PBS and the fusion protein was eluted using 0.1M Tris-HCl pH 8.0, 150mM NaCl, 1mM EDTA, and 20mM glutathione (reduced form). The protein was then further purified by gel filtration on a Superdex200 26/60 (Pharmacia) column, previously equilibrated in 50mM Tris-HCl pH 8.0, 150mM NaCl, and 1mM EDTA, and subsequently subjected to thrombin digest (1U thrombin/mg protein) for 3 hours at 20°C. $NarX_{S2}$ was then purified from the cleaved GST by gel filtration on a Superdex75 26/60 (Pharmacia), previously equilibrated with 20mM Tris-HCl pH 7.5, 50mM NaCl, and 1mM EDTA. The purified protein appeared homogenous by SDS-PAGE and native PAGE, and was concentrated to ~40mg/ml for crystallization.

Crystallization

Sodium nitrate from a 1M stock was added to $NarX_{S1}$ to a final concentration of 5mM before crystallization. Crystals of $NarX_{S1}(NO_3)$ were grown by hanging drop vapor diffusion against a buffer containing 0.1M Tris-HCl pH 8.5 and 2M $NH_4H_2PO_4$ at 4°C with a protein to reservoir buffer ratio of 1:1. Large prism-shaped single crystals up to 600μm in length appeared after four days. The crystals were serially soaked in crystallization buffer supplemented with gradually increasing glycerol concentrations from 5% to 20% prior to freezing in liquid nitrogen.

Crystals of $NarX_{S2}$(apo) were grown by hanging drop vapor diffusion against 23% polyethylene glycol (PEG) 3350, 1% isopropanol, and 0.1M HEPES pH 7.5 at 4°C. The protein concentration used was 20mg/ml and the protein to reservoir buffer ratio was 1:1. Clusters of plates appeared after two days, and slowly increased in thickness and size over a period of two weeks. Plate fragments were initially soaked in crystallization buffer

supplemented with a mixture of 5% glycerol and 5% ethylene glycol, and then finally in 10% glycerol and 10% ethylene glycol prior to freezing in liquid nitrogen.

Although crystals of $NarX_{S1}$ could not be grown without the presence of nitrate, crystals of $NarX_{S2}$ could be grown in the presence of nitrate in a different condition than that required for the crystallization of $NarX_{S1}$. Such crystals appeared to be of a different morphology than the nitrate-complexed $NarX_{S1}$ crystals; however, due to their small size and difficulties in their reproducibility, they were not used for diffraction experiments.

Structure Determination

$NarX_{S1}$ in Complex with Nitrate—MAD data from four wavelengths at the Se K-edge were collected from a single frozen SeMet $NarX_{S1}(NO_3)$ crystal at the X4A beamline of the NSLS (National Synchrotron Light Source) at Brookhaven National Laboratory. Data to 2.0Å spacings (170mm detector distance) were collected using 1° oscillations of 6s exposure times. Because of numerous overloads, a low-angle MAD data set was also collected to ~3.5Å spacings (375mm detector distance) using 4° oscillations of 4s exposure times. A final high-angle data set extending to 1.7Å spacings (130mm detector distance) was collected with an exposure time of 21s at the edge wavelength from the same crystal, using 0.8° oscillations to minimize overlaps. The data were indexed and merged using Denzo and Scalepack of the HKL program package (Otwinowski and Minor, 1997). Initial phases were calculated using Solve (Terwilliger and Berendzen, 1999) in each possible space group ($P4_12_12$ and $P4_32_12$) and improved by solvent flattening using DM (Cowtan, 1994) of the CCP4 program package (Bailey, 1994). Visual inspection of the resulting electron density maps at 2.2Å resolution confirmed $P4_32_12$ as the correct space group. A figure of merit of 0.67 was obtained from phasing and refinement of seven selenium sites found in the two molecules of the asymmetric unit, and after solvent flattening, the figure of merit rose to 0.82. Phasing was then extended to 1.7Å spacings using DM (Cowtan, 1994) against the high angle dataset collected at the edge wavelength. The model was almost entirely built using Arp/Warp 5.1 (Perrakis et al., 1999) and missing residues (8% of the final model) were manually built in O (Jones et al., 1991). The model was then refined against the high angle dataset in CNS (Brunger et al., 1998) using iterative cycles of simulated annealing, conjugate gradient minimization, temperature-factor refinement, and manual rebuilding. Diffraction data and refinement statistics are listed in Tables 3.1 and 3.2 respectively.

$NarX_{S2}$ in the Apo State—A native dataset to 1.7Å spacings (140mm detector distance) from a single frozen crystal of $NarX_{S2}$(apo) was collected at X4A of the NSLS at Brookhaven National Labs using 1° oscillations with 30s exposure times. Due to overloaded reflections, a low resolution dataset was collected from the same crystal to ~3.2Å spacings (300mm detector distance) using 3° oscillations and 15s exposure times. The data was indexed, merged, and processed using the HKL program package (Otwinowski and Minor, 1997) and the CCP4 program suite (Bailey, 1994) in space group P1. According to Matthew's coefficient calculations (Matthews, 1968), the unit cell most likely contained either 3 or 4 molecules. Using residues 42 to 148 of the refined $NarX_{S1}(NO_3)$ structure as a molecular replacement search model, cross-rotation and translation function searches were performed in CNS (Brunger et al., 1998) to locate and fix the position of an initial molecule. The positions of three additional molecules were subsequently located by fixing the position of an initial molecule and then performing additional cycles of cross-rotation and translation searches to find them in iteration. Arp/Warp 6.0 (Perrakis et al., 1999) was used for model improvement and re-tracing of the apo structure, and refinement was performed using O (Jones et al., 1991) and CNS (Brunger et al., 1998) in the same manner as outlined before. Diffraction data and refinement statistics are also listed in Tables 3.1 and 3.2 respectively.

Acknowledgments

We thank Craig Ogata, Randy Abramowitz, and Alberto Marina for help with synchrotron data collection. This work was supported in part by NIH grant GM34102. Beamline X4A of the National Synchrotron Light Source (NSLS) at Brookhaven National Laboratory, a DOE facility, is supported by the New York Structural Biology Center.

References

Appleman JA, Chen LL, Stewart V. Probing conservation of HAMP linker structure and signal transduction mechanism through analysis of hybrid sensor kinases. J Bacteriol. 2003; 185:4872–4882. [PubMed: 12897007]

Bailey S. The CCP4 suite - programs for protein crystallography. Acta Crystallogr D. 1994; 50:760–763. [PubMed: 15299374]

Biemann HP, Koshland DE. Aspartate Receptors of Escherichia-Coli and Salmonella-Typhimurium Bind Ligand with Negative and Half-of-the-Sites Cooperativity. Biochemistry. 1994; 33:629–634. [PubMed: 8292590]

Brunger AT, Adams PD, Clore GM, DeLano WL, Gros P, Grosse-Kunstleve RW, Jiang JS, Kuszewski J, Nilges M, Pannu NS, et al. Crystallography & NMR system: A new software suite for macromolecular structure determination. Acta Crystallogr D. 1998; 54:905–921. [PubMed: 9757107]

Cavicchioli R, Chiang RC, Kalman LV, Gunsalus RP. Role of the periplasmic domain of the *Escherichia coli* NarX sensor-transmitter protein in nitrate-dependent signal transduction and gene regulation. Mol Microbiol. 1996; 21:901–911. [PubMed: 8885262]

Chervitz SA, Falke JJ. Molecular mechanism of transmembrane signaling by the aspartate receptor: A model. Proc Natl Acad Sci USA. 1996; 93:2545–2550. [PubMed: 8637911]

Chiang RC, Cavicchioli R, Gunsalus RP. 'Locked-on' and 'locked-off' signal transduction mutations in the periplasmic domain of the *Escherichia coli* NarQ and NarX sensors affect nitrate- and nitrite-dependent regulation by NarL and NarP. Mol Microbiol. 1997; 24:1049–1060. [PubMed: 9220011]

Cho US, Bader MW, Amaya MF, Daley ME, Klevit RE, Miller SI, Xu WQ. Metal bridges between the PhoQ sensor domain and the membrane regulate transmembrane signaling. J Mol Biol. 2006; 356:1193–1206. [PubMed: 16406409]

Chothia C, Lesk AM. Helix movements in proteins. Trends Biochem Sci. 1985; 10:116–118.

Cowtan K. CCP4/ESF-EACBM Newsletter on Protein. Crystallography. 1994; 31:34–38.

Dutta R, Qin L, Inouye M. Histidine kinases: diversity of domain organization. Mol Microbiol. 1999; 34:633–640. [PubMed: 10564504]

Esnouf RM. An extensively modified version of MolScript that includes greatly enhanced coloring capabilities. J Mol Graph Mod. 1997; 15:132.

Falke JJ, Hazelbauer GL. Transmembrane signaling in bacterial chemoreceptors. Trends Biochem Sci. 2001; 26:257–265. [PubMed: 11295559]

Garrity LF, Ordal GW. Activation of the CheA kinase by asparagine in *Bacillus subtilis* chemotaxis. Microbiology. 1997; 143:2945–2951. [PubMed: 12094812]

Goh EB, Bledsoe PJ, Chen LL, Gyaneshwar P, Stewart V, Igo MM. Hierarchical control of anaerobic gene expression in *Escherichia coli* K-12: the nitrate-responsive NarX-NarL regulatory system represses synthesis of the fumarate-responsive DcuS-DcuR regulatory system. J Bacteriol. 2005; 187:4890–4899. [PubMed: 15995204]

Grasberger B, Minton AP, Delisi C, Metzger H. Interaction between Proteins Localized in Membranes. Proc Natl Acad Sci USA. 1986; 83:6258–6262. [PubMed: 3018721]

Hendrickson WA. Transformations to Optimize the Superposition of Similar Structures. Acta Crystallogr Sect A. 1979; 35:158–163.

Holm L, Sander C. Protein-Structure Comparison by Alignment of Distance Matrices. J Mol Biol. 1993; 233:123–138. [PubMed: 8377180]

Iuchi S, Lin EC. Adaptation of Escherichia coli to respiratory conditions: regulation of gene expression. Cell. 1991; 66:5–7. [PubMed: 2070418]

Jones TA, Zou JY, Cowan SW, Kjeldgaard M. Improved methods for building protein models in electron-density maps and the location of errors in these models. Acta Crystallogr A. 1991; 47:110–119. [PubMed: 2025413]

Kaiser M, Sawers G. Nitrate repression of the *Escherichia coli* pfl operon is mediated by the dual sensors NarQ and NarX and the dual regulators NarL and NarP. J Bacteriol. 1995; 177:3647–3655. [PubMed: 7601827]

Kleywegt GJ, Jones TA. A super position. CCP4/ESF-EACBM Newsletter on Protein. Crystallography. 1994; 31:9–14.

Kraulis PJ. Molscript - a program to produce both detailed and schematic plots of protein structures. J Appl Crystallogr. 1991; 24:946–950.

Lee AI, Delgado A, Gunsalus RP. Signal-dependent phosphorylation of the membrane-bound NarX two-component sensor-transmitter protein of Escherichia coli: nitrate elicits a superior anion ligand response compared to nitrite. J Bacteriol. 1999; 181:5309–5316. [PubMed: 10464202]

Lin HY, Bledsoe PJ, Stewart V. Activation of yeaR-yoaG operon transcription by the nitrate-responsive regulator NarL is independent of oxygen- responsive regulator Fnr in *Escherichia coli* K-12. J Bacteriol. 2007; 189:7539–7548. [PubMed: 17720788]

Matthews BW. Solvent content of protein crystals. J Mol Biol. 1968; 33:491–497. [PubMed: 5700707]

Metzger H. Transmembrane signaling - the joy of aggregation. J Immunol. 1992; 149:1477–1487. [PubMed: 1324276]

Ottemann KM, Xiao WZ, Shin YK, Koshland DE. A piston model for transmembrane signaling of the aspartate receptor. Science. 1999; 285:1751–1754. [PubMed: 10481014]

Otwinowski Z, Minor W. Processing of X-ray diffraction data collected in oscillation mode. Methods Enzymol. 1997; 276:307–326.

Pappalardo L, Janausch IG, Vijayan V, Zientz E, Junker J, Peti W, Zweckstetter M, Unden G, Griesinger C. The NMR structure of the sensory domain of the membranous two-component fumarate sensor (histidine protein kinase) DcuS of Escherichia coli. J Biol Chem. 2003; 278:39185–39188. [PubMed: 12907689]

Perrakis A, Morris R, Lamzin VS. Automated protein model building combined with iterative structure refinement. Nature Struct Biol. 1999; 6:458–463. [PubMed: 10331874]

Reinelt S, Hofmann E, Gerharz T, Bott M, Madden DR. The structure of the periplasmic ligand-binding domain of the sensor kinase CitA reveals the first extracellular PAS domain. J Biol Chem. 2003; 278:39189–39196. [PubMed: 12867417]

Robinson VL, Buckler DR, Stock AM. A tale of two components: a novel kinase and a regulatory switch. Nature Struct Biol. 2000; 7:626–633. [PubMed: 10932244]

Russo FD, Silhavy TJ. The essential tension: opposed reactions in bacterial two-component regulatory systems. Trends Microbiol. 1993; 1:306–310. [PubMed: 8162415]

Schneider TR. Objective comparison of protein structures: error-scaled difference distance matrices. Acta Crystallogr D. 2000; 56:714–721. [PubMed: 10818348]

Schneider TR. A genetic algorithm for the identification of conformationally invariant regions in protein molecules. Acta Crystallogr D. 2002; 58:195–208. [PubMed: 11807243]

Schroder I, Wolin CD, Cavicchioli R, Gunsalus RP. Phosphorylation and dephosphorylation of the NarQ, NarX, and NarL proteins of the nitrate-dependent two-component regulatory system of *Escherichia coli*. J Bacteriol. 1994; 176:4985–4992. [PubMed: 8051011]

Sheriff S, Hendrickson WA, Smith JL. Structure of myohemerythrin in the azidomet state at 1.7/1.3-Å resolution. J Mol Biol. 1987; 197:273–296. [PubMed: 3681996]

Stewart V. Nitrate regulation of anaerobic respiratory gene expression in *Escherichia coli*. Mol Microbiol. 1993; 9:425–434. [PubMed: 8412692]

Stewart V. Biochemical Society Special Lecture. Nitrate- and nitrite-responsive sensors NarX and NarQ of proteobacteria. Biochem Soc Trans. 2003; 31:1–10. [PubMed: 12546643]

Stock AM, Robinson VL, Goudreau PN. Two-component signal transduction. Ann Rev Biochem. 2000; 69:183–215. [PubMed: 10966457]

Szurmant H, Bunn MW, Cho SH, Ordal GW. Ligand-induced conformational changes in the Bacillus subtilis chemoreceptor McpB determined by disulfide crosslinking in vivo. J Mol Biol. 2004; 344:919–928. [PubMed: 15544802]

Terwilliger TC, Berendzen J. Automated MAD and MIR structure solution. Acta Crystallogr D. 1999; 55:849–861. [PubMed: 10089316]

Thompson JD, Higgins DG, Gibson T. Clustal-W - Improving the sensitivity of progressive multiple sequence alignment through sequence weighting, position-specific gap penalties and weight matrix choice. Nucl Acids Res. 1994; 22:4673–4680. [PubMed: 7984417]

Utsumi R, Brissette RE, Rampersaud A, Forst SA, Oosawa K, Inouye M. Activation of Bacterial Porin Gene-Expression by a Chimeric Signal Transducer in Response to Aspartate. Science. 1989; 245:1246–1249. [PubMed: 2476847]

Ward SM, Bormans AF, Manson MD. Mutationally altered signal output in the nart (NarX-Tar) hybrid chemoreceptor. J Bacteriol. 2006; 188:3944–3951. [PubMed: 16707686]

Ward SM, Delgado A, Gunsalus RP, Manson MD. A NarX-Tar chimera mediates repellent chemotaxis to nitrate and nitrite. Mol Microbiol. 2002; 44:709–719. [PubMed: 11994152]

West AH, Stock AM. Histidine kinases and response regulator proteins in two-component signaling systems. Trends Biochem Sci. 2001; 26:369–376. [PubMed: 11406410]

Williams SB, Stewart V. Discrimination between structurally related ligands nitrate and nitrite controls autokinase activity of the NarX transmembrane signal transducer of Escherichia coli K-12. Mol Microbiol. 1997; 26:911–925. [PubMed: 9426129]

Wolanin PM, Thomason PA, Stock JB. Histidine protein kinases: key signal transducers outside the animal kingdom. Genome Biol. 2002; 3 Reviews 3013.1–3013.8.

Xu Q, Black WP, Mauriello EM, Zusman DR, Yang Z. Chemotaxis mediated by NarX-FrzCD chimeras and nonadapting repellent responses in *Myxococcus xanthus*. Mol Microbiol. 2007; 66:1370–1381. [PubMed: 18028315]

Xu Q, Black WP, Ward SM, Yang Z. Nitrate-dependent activation of the Dif signaling pathway of *Myxococcus xanthus* mediated by a NarX-DifA interspecies chimera. J Bacteriol. 2005; 187:6410–6418. [PubMed: 16159775]

Yeh JI, Biemann HP, Prive GG, Pandit J, Koshland DE, Kim SH. High-resolution structures of the ligand binding domain of the wild-type bacterial aspartate receptor. J Mol Biol. 1996; 262:186–201. [PubMed: 8831788]

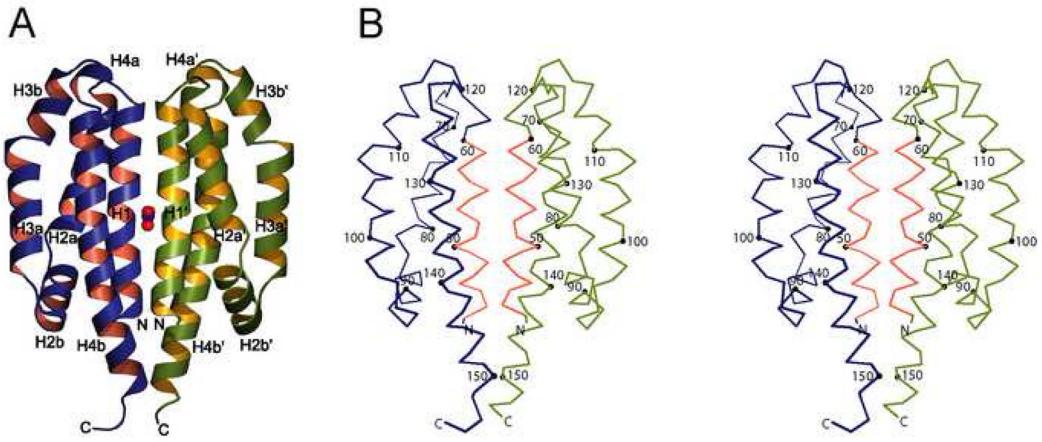

Figure 1. Structure of NarX$_S$ in complex with nitrate

(A) Ribbon diagram with secondary structure elements labeled appropriately. Nitrate is depicted in ball-and-stick representation with nitrogen colored blue and oxygen colored red. (B) A stereo plot of the Cα trace. Every tenth Cα atom is depicted as a black sphere and labeled accordingly. The P-box region (Cavicchioli et al., 1996) in the first helix of each protomer is shown in red. Nitrate was omitted for clarity. Drawings were made with MolScript (Kraulis, 1991) and BobScript (Esnouf, 1997).

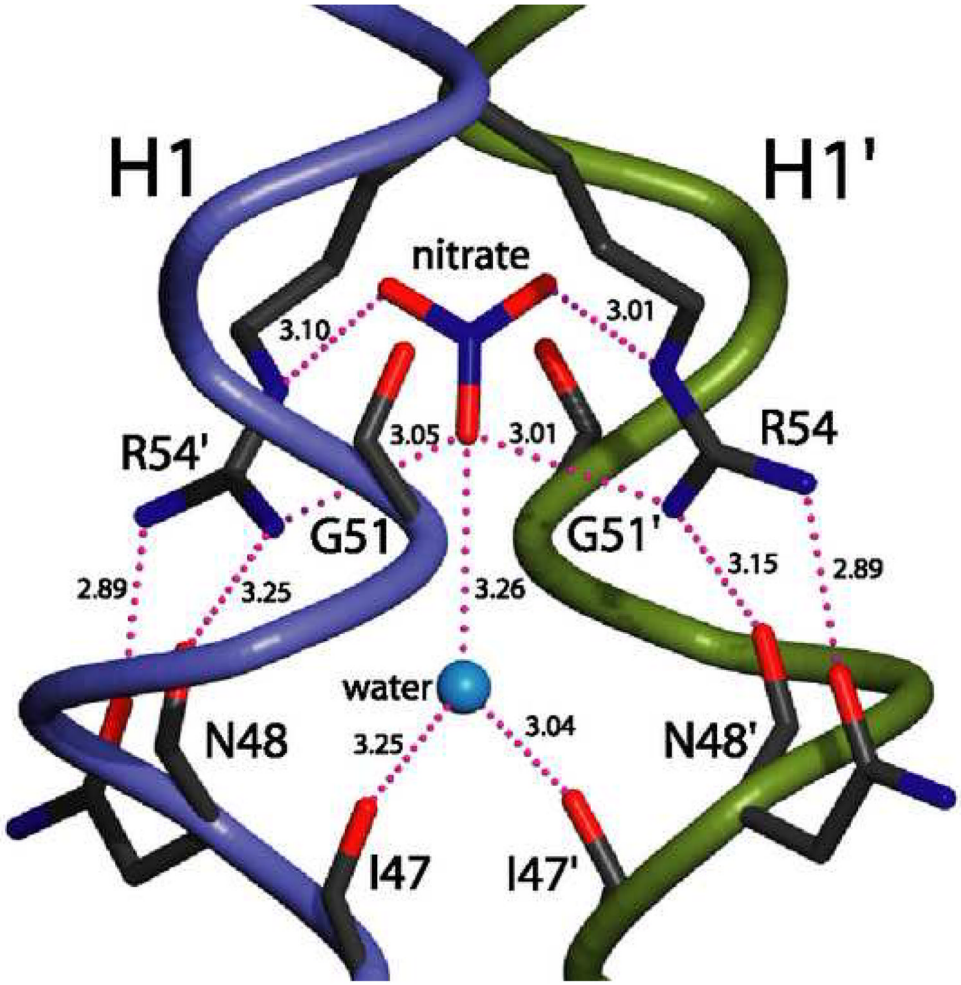

Figure 2. Nitrate-binding site

The protein backbone of helices H1 and H1′ are shown in worm representation with residues at the nitrate-binding site depicted in stick representation and labeled accordingly. Atoms are colored black, red, and blue for carbon, oxygen, and nitrogen respectively. Water is depicted as a light blue sphere. Hydrogen bonds (red dotted lines) are labeled with distances (Å).

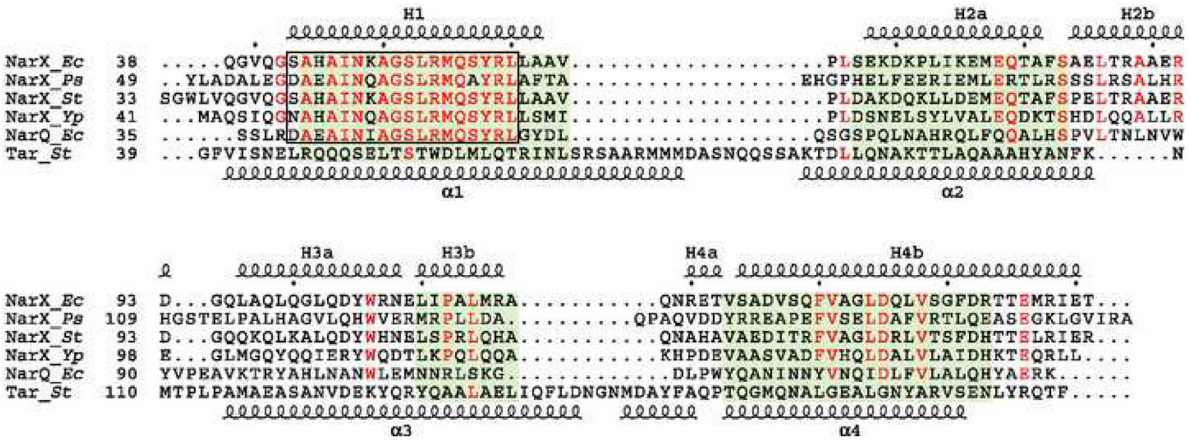

Figure 3. Structure-based sequence alignment of NarX, NarQ, and Tar

The sequences of the periplasmic domains of NarX and Tar are aligned and numbered accordingly. The secondary structure elements of NarX and Tar are shown and labeled above and below the sequences respectively. The P-box region of NarX (Cavicchioli et al., 1996) is indicated by a black rectangle. Conserved residues are shown in red, structurally aligned residues are highlighted in green, and organism names are abbreviated in italics (*Ec* for *Escherichia coli*, *Ps* for *Pseudomonas stutzeri*, *St* for *Salmonella typhimurium*, and *Yp* for *Yersinia pestis*). Structural alignment is assigned when at least three contiguous Cα positions of NarX are within 3.0Å of Tar counterparts.

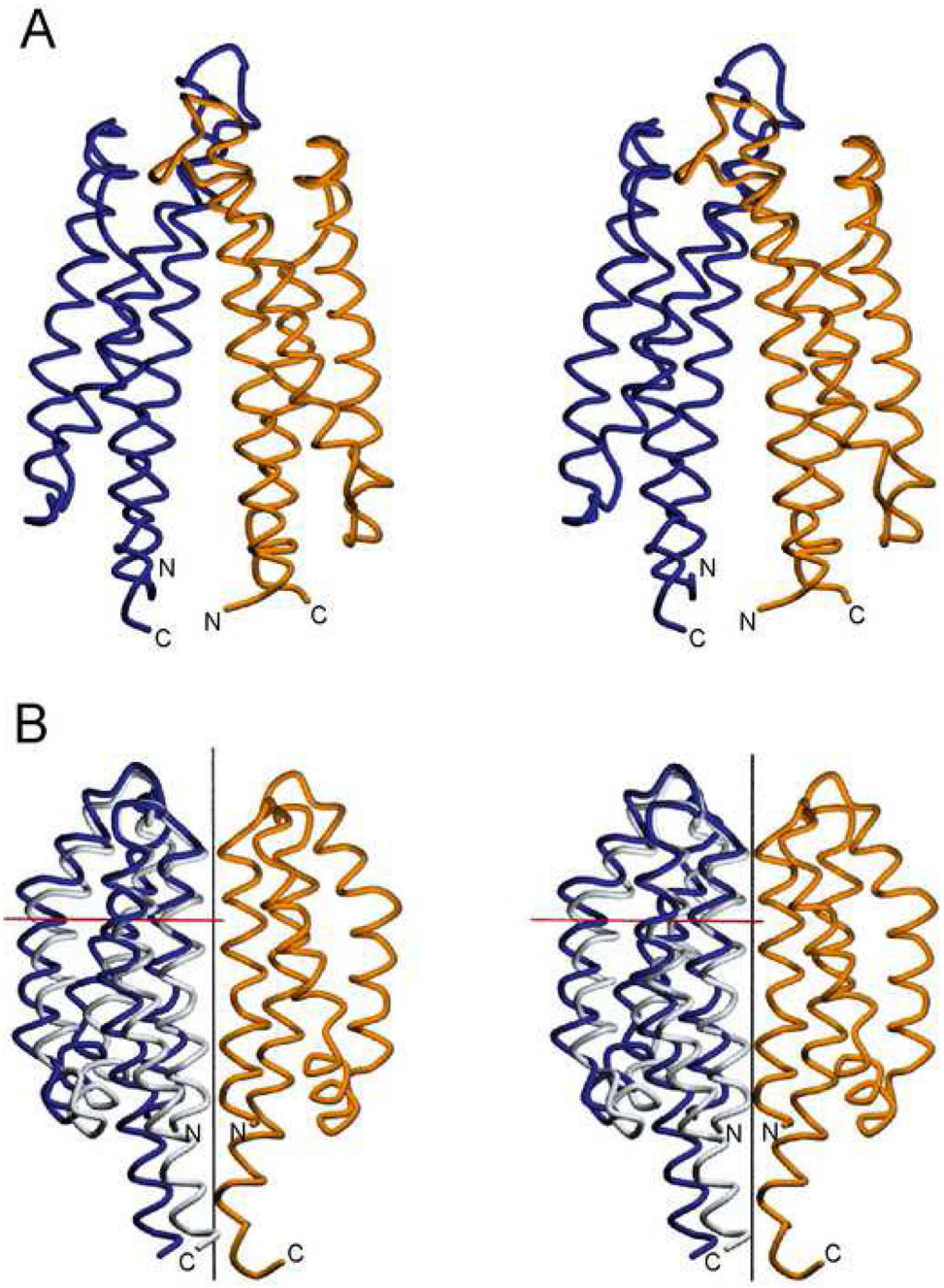

Figure 4. Comparison of $NarX_S$ and Tar dimers

(A) Worm representation of the dimeric aspartate receptor Tar, drawn in stereo. Subunits A and B of Tar (Yeh et al., 1996) are colored yellow and blue respectively. (B) Worm representation of $NarX_{s1}$ dimers in stereo. A 'Tar-like' $NarX_s$ dimer is formed when subunits A (yellow) and B (blue) from $NarX_{s1}(NO_3)$ are independently superimposed upon subunits A and B of Tar, respectively. Subunit B from the natural $NarX_s$ dimer of Fig. 1 is shown in grey. The black vertical line represents the quasi two-fold rotation axis of the observed dimer. The red line shows the resulting axis of 9.3° rotation that relates B subunits from the natural, observed $NarX_S$ dimer and the constructed 'Tar-like' $NarX_s$ dimer. In the

orientation of the molecules shown, the red rotation axis intersects the black rotation axis and is angled approximately 30 degrees above the plane of the figure.

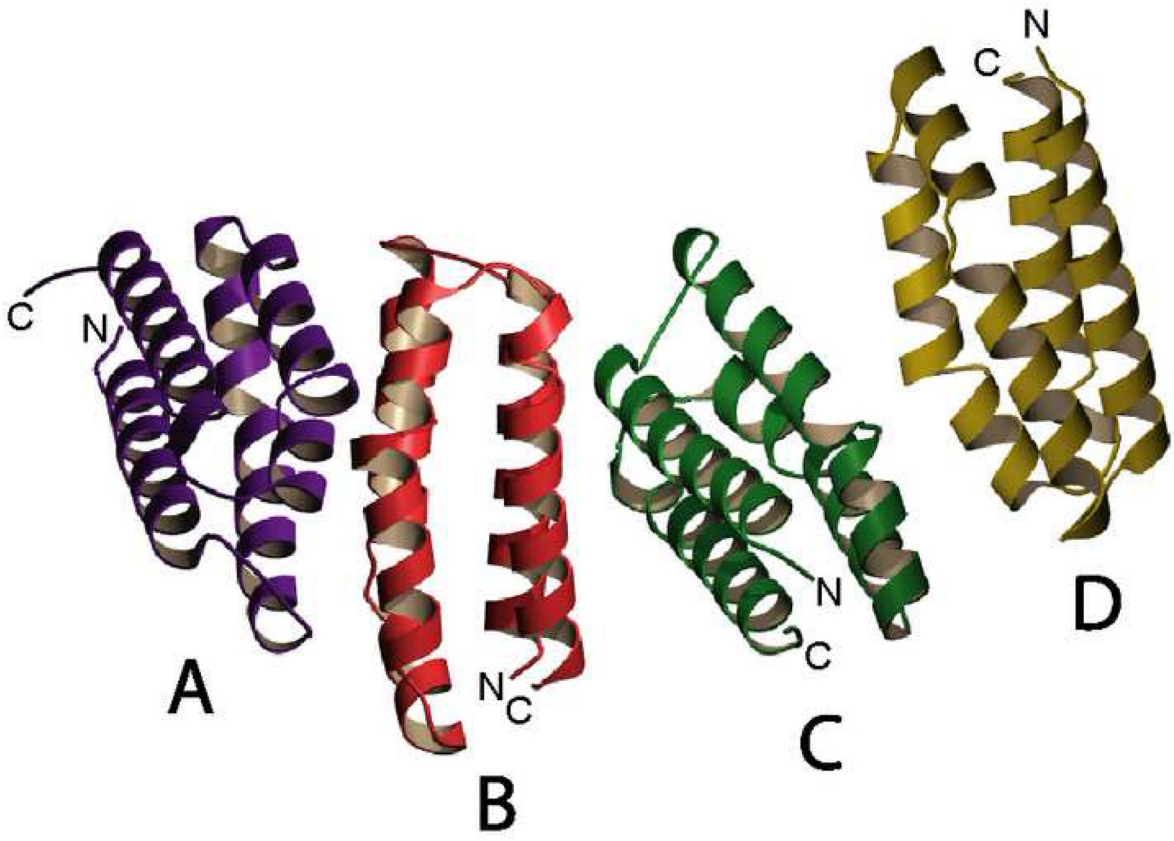

Figure 5. Structure of $NarX_S$(apo)

The overall structure of $NarX_{S2}$ in a nitrate-free state is shown as a ribbon diagram. Each monomer is colored and labeled individually.

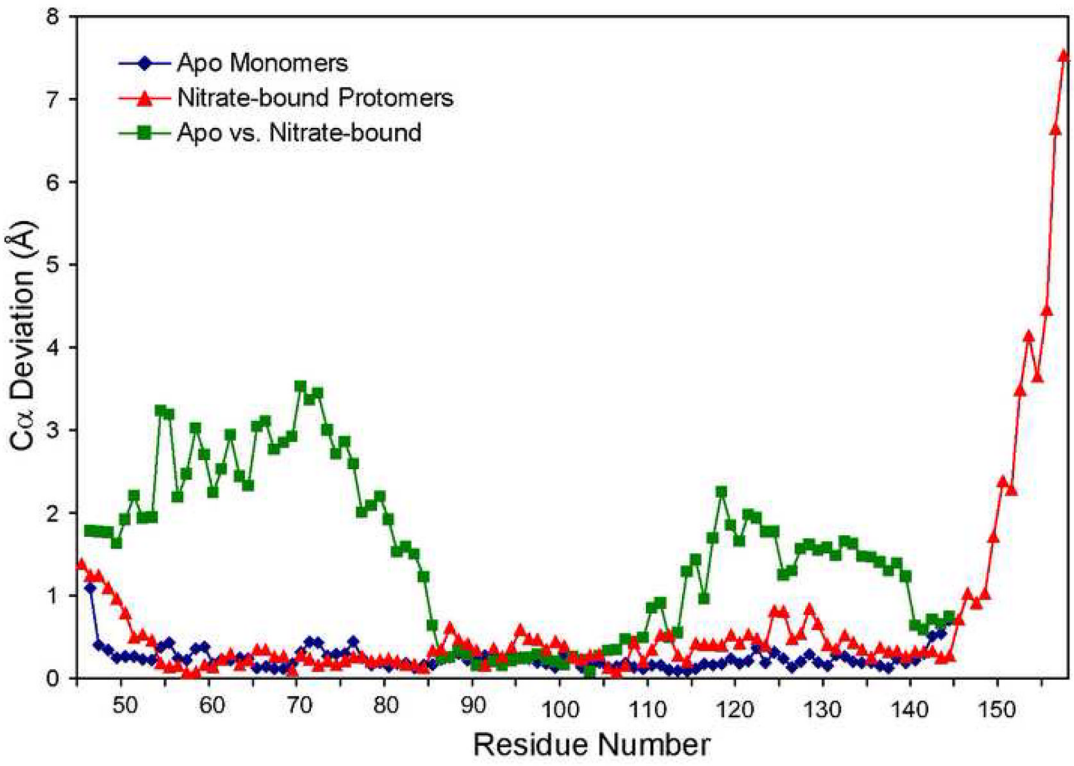

Figure 6. Intermolecular Cα deviations of superimposed NarX molecules

Residue number is plotted on the horizontal axis and intermolecular Cα deviation is plotted on the vertical axis. The blue graph represents the average of all Cα distances between pairwise superimposition (residues 47 - 51 and 57 - 141) of all four $NarX_{S2}$(apo) molecules. The red graph represents Cα distances between the superimposed (residues 47 - 115) $NarX_{S1}(NO_3)$ protomers. The green graph represents the average of Cα deviations between pairwise superimpositions (residues 83 - 106) of each nitrate-bound protomer with each apo monomer.

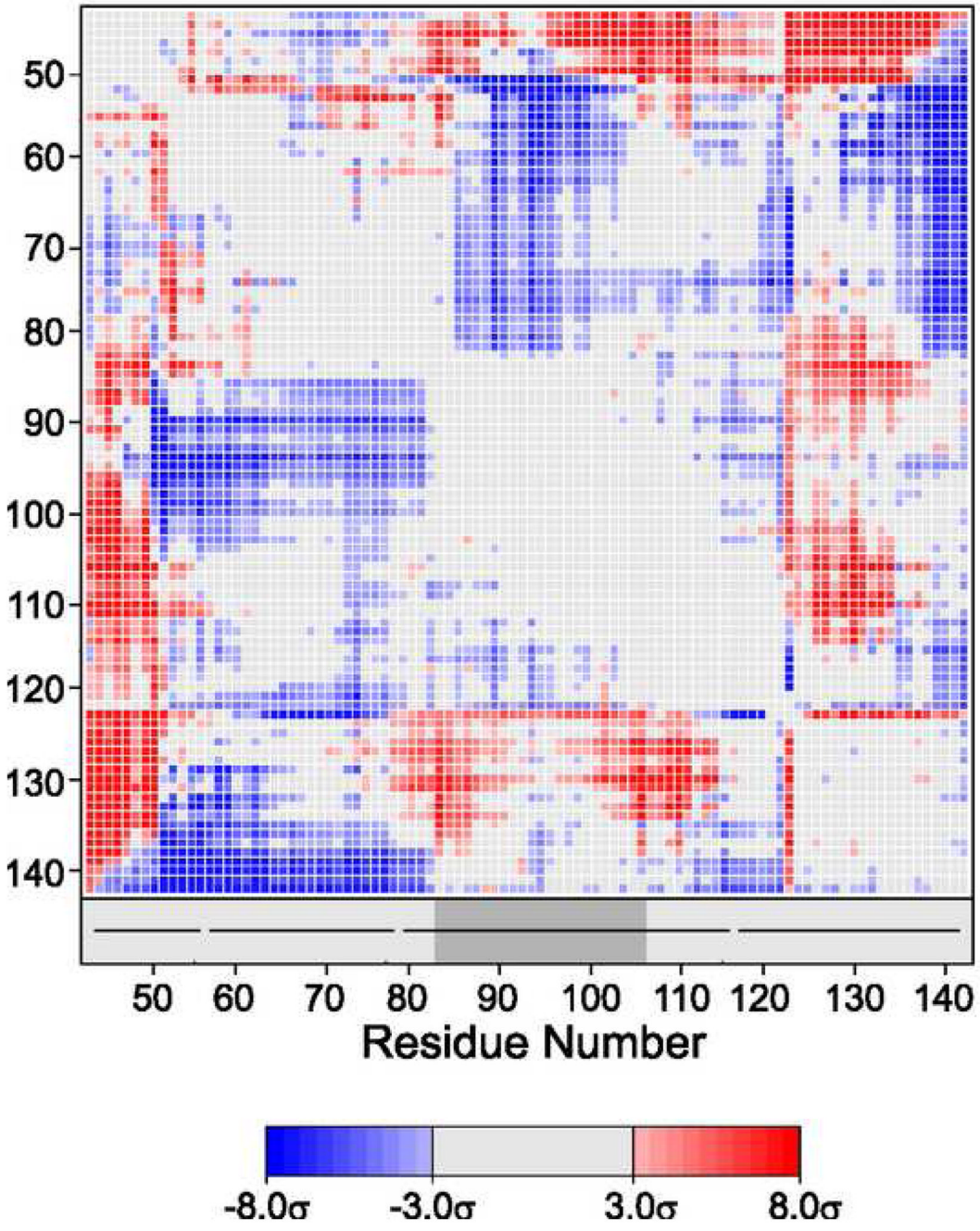

Figure 7. Difference distance matrix

An ESCET (Schneider, 2000; Schneider, 2002) error-scaled difference distance matrix calculated for molecules of NarX in the apo and nitrate-bound states. Regions of conformational variance (red and blue) and invariance (white) are colored according to the magnitude of their difference. The program identified residues 83 to 106 (highlighted in gray) to be a structurally invariant region common to all molecules at the 3σ level. White 'blocks' along the diagonal of the matrix correspond to the positions of the helices in the structures, and flexible regions between H2a and H2b, and H3a and H3b allow the relative orientations of these helices to shift as rigid bodies with respect to each other. Residues in the upper portion of H1 and H2a (residues 60-70), and the H1-H2a loop (residues 103-119)

are conformationally invariant with respect to each other, and they appear to move together as a rigid unit.

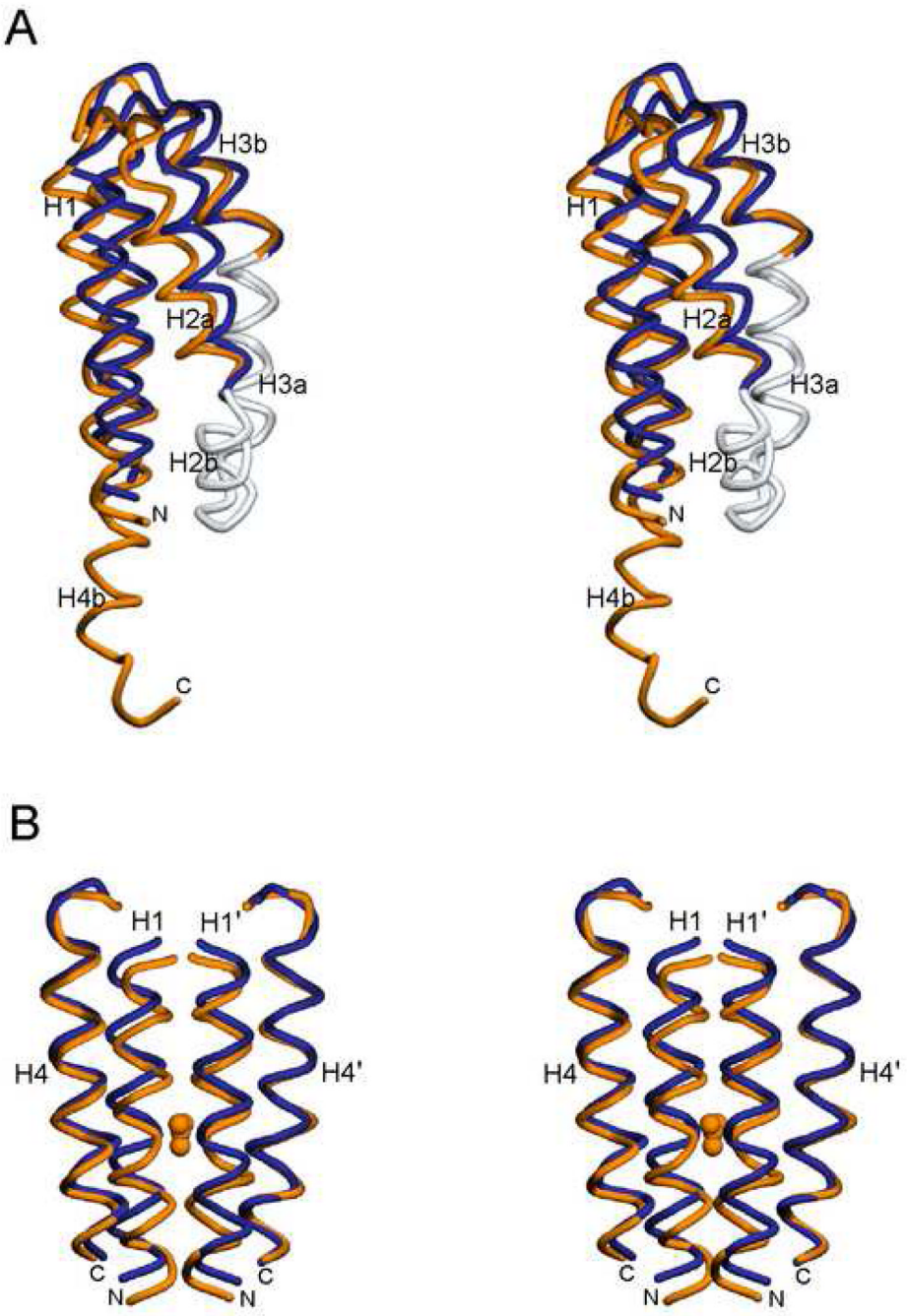

Figure 8. Superimposition of NarX in nitrate-bound and apo states

(A) Nitrate-bound NarX protomer A is shown superimposed with apo-state NarX molecule B and are both depicted in worm representation. Conformationally variant regions of the nitrate-bound and apo structures are colored gold and blue, respectively. Conformationally invariant Cα positions of residues 83 to 106 are superimposed and colored light gray. (B) A model of a dimeric apo state (blue) is created by superimposition of Cα positions of residues 83 to 106 of the apo state monomer B upon nitrate-bound protomers A and A′ (gold), showing a piston-type displacement between the N- and C-terminal helices upon binding of nitrate. Only residues of the N- and C-terminal helices from residues 43 to 62 and 120 to

151 of each signaling state are shown for greater clarity, and the location of the single bound nitrate ion is shown in gold in CPK representation. Drawings are in stereo.

Table 1

NarX diffraction data

Data Set	d_{min} (Å)	Wavelength (Å)	No. of Ref'ns	Average Redundancy	<I>/(δ)	Completeness (%) [a]	R_{merge} (%) [b]
$NarX_{S2}$ (apo)	1.7	0.9795	37137	1.4	13.8	92.3 (78.5)	5.0 (35.2)
Se $NarX_{S1}$ (NO_3)	1.7	0.9794 (high angle)	27197 [c]	4.5	20.1	98.4 (99.0)	4.6 (25.0)
Se $NarX_{S1}$ λ1 (NO_3)	2.0	0.9904 (low remote)	30941 [d]	4.1	10.1	99.2 (99.6)	5.8 (25.8)
Se $NarX_{S1}$ λ2 (NO_3)	2.0	0.9794 (edge)	30992	4.2	9.9	99.3 (99.6)	6.1 (28.0)
Se $NarX_{S1}$ λ3 (NO_3)	2.0	0.9786 (peak)	31011	4.2	9.1	99.3 (99.6)	6.8 (35.8)
Se $NarX_{S1}$ λ4 (NO_3)	2.0	0.9673 (high remote)	30963	4.2	8.2	99.1 (99.6)	7.8 (39.1)

[a] Values in outermost shell are given in parentheses.

[b] $R_{merge} = (\Sigma|I_i - < I_i >|)/\Sigma|I_i|$, where I_i is the integrated intensity of a given reflection.

[c] Bijvoet mates are treated as if identical.

[d] Bijvoet mates are treated as unique reflections.

Table 2

NarX refinement statistics

Parameter	$NarX_{S1}$ (NO_3)	$NarX_{S2}$ (apo)
Bragg Spacings (Å)	25 – 1.7	20 – 1.7
Space Group	$P4_32_12$	P1
Cell Parameters a, b, c (Å)/α, β, γ (°)	55.76, 55.76, 155.26 90, 90, 90	28.24, 39.82, 83.95 80.76, 89.57, 85.29
Z_a [a]	2	4
Solvent Content (%)	43.2	37.0
R_{work} [b]	0.217	0.189
R_{free} [c]	0.258	0.239
Number of Reflections	27155	36888
Number of total atoms (non-hydrogen)	2079	3945
Number of protein atoms	1820	3499
Number of ligand atoms	4 (nitrate)	8 (isopropanol)
Number of waters	255	438
Average B factor	32.6	23.1
RMS Bonds	0.017	0.015
RMS Angles	1.7	1.5
PDB Code	3EZH	3EZI

[a] Z_a stands for number of molecules per asymmetric unit.

[b] $R_{work} = (\Sigma ||F_O| - |F_C||)/\Sigma|F_O|$, where F_O and F_C denote observed and calculated structure factors respectively.

[c] R_{free} was calculated using 5% of data excluded from refinement.